
Worldwide
EMATEM
European Metrology Association
for Thermal Energy Measurement

Q-Sweep

Flow spectral measurement principle

1rst part: **Ematem Summer school 2021-2022; principle**
2nd part: **Ematem Summer school 2023; measurement (cont.)**

Project Initiator, test facility development and measurements:
Alexander Rombach

Elaboration and Presentation:
Humphrey Spoor

***Interactive presentation*:**

short questions / something not clear / short elucidations

please do interrupt **(English / German / French / Dutch)** ***!!***

Summary

Flow spectral analysis, realised by means of a dual / quadruple piston prover calibration system with infinite volume

- Short recapitulation part-1 (excerpt 2022):
  - goal / physics background / layout / boundary / start conditions
  - DAQ (data acquisition) / DP (data processing)
  - resolution / minimum test volume
  - system (rig ⇔ DUT) inertia interaction (flow change rig ⇔ slew rate DUT)

- Part-2:
  - measurement results till now
  - uncertainty analysis (in development)
  - traceability (in development)
  - conclusions part-2

EMATEM

Physical background, volume flow spectrum

- Flow (English) ≡ volume rate, in [m^3/s], as per definition rate ≡ per second. Flow rate ≡ change in flow per second, so a flow acceleration in [$m^3/s/s$]. Flow rate (USA) = double Dutch.
- The systems & signals principle of spectral analysis is assumed to be known. In the time-frequency domain the pair (t,ω) [s,Hz] is used; in the spatial domain the pair (λ,k) [m,m^{-1}] is used (e.g., spatial filtering in optics). For the flow setup it will become the pair ($\phi_V/p,p/\phi_V$) [$m^3/s,s/m^3$]. In other words, the time domain is represented by the DUT-output quantity (turbine: volume flow per pulse) or whatever quantity is characteristic applicable; e.g., delta-TOF in ultrasonics.
- By means of a continuous increase respectively a decrease in flow, constantly smaller (larger) partial measurements are registered, synchronously with the meter (DUT) pulse output. If these increments / decrements are chosen too small, there will be an inertia lag; a resolution issue (aliasing).

So for each specific measuring principle and specific measurement setup of a test object, the slew rate and resolution should be selected in combination, in order to suit each other well. Consequently, it is recommended to integrate live monitoring of these values in the SW.

Slew rate (1)

The slew rate (maximum time lag) in electronics is defined as:

$$SR_e\left[V/\mu s\right] \equiv \frac{\text{maximum voltage difference}\left[V\right]}{\text{rising time}\left[s\right]} = \left|\frac{dV_{max}(t)}{dt}\right|$$

Hydrodynamical analogue defined:

$$SR_p\left[Pa/s\right] \equiv \frac{\text{maximum pressure variation}\left[Pa\right]}{\text{rising time}\left[s\right]} = \left|\frac{dp_{max}(t)}{dt}\right|$$

The Joukowski expression for acoustical wave propagation in tubes:

$$\Delta p = \rho\, c\, \hat{u} = \frac{\rho\, c\, Q_V}{A} \propto Q_V$$

ρ = medium density (kg/m^3)
c = medium sound velocity (m/s)
$\hat{u}$ = the flow velocity amplitude (m/s)
ϕ_V = flow amplitude (l/h)
A = tube cross section (m^2)

Slew rate (2)

Intermezzo: Joukowski linearisation:

$$\Delta\left(\Delta\tilde{p}\right) = \tfrac{1}{2}\,\rho\,\Delta\left(c+\tilde{u}\right)^2 = \tfrac{1}{2}\,\rho\,\Delta\left(c^2+\tilde{u}^2+2c\,\tilde{u}\right) \approx \rho\,c\,\tilde{u} = \frac{\rho\,c\,\tilde{Q}_V(t)}{A} \propto \Delta Q_V$$

so:

$$SR_q\left[l/s^2\right] \equiv \frac{\text{maximum flow variation}\left[l/s\right]}{\text{rising time}\left[s\right]} = \left|\frac{dQ_V(t)}{dt}\right|$$

per definition:

$$f_{out}\left[Hz\right] = PC\left[p/m^3\right] * Q_V\left[m^3/s\right]$$

Slew rate (3)

The result is:

$$SR_q\left[m^3/s^2\right] \equiv \left|\frac{dQ_V(t)}{dt}\right| = \frac{1}{PC}\frac{\Delta f_{out}}{\Delta t}$$

the maximal allowable sweep frequency $\Delta f/\Delta t$ follows from the manufacturer data:

- Primary Constant (PC) in [p/l]
- slew rate in [m^3/s^2], or more practical [l/h/s], but are these data available ???

Evident: for a faster response a higher resolution of the underlying physical measurement principle is needed.

Measurement conditions demands

Important for measurement stability:

- constant room temperature stability
- double walls through which temperature control water flows
- constant pressure conditions without pressure surges when changing pistons
- smooth piston calibrated transition movement
- upstream fully-developed flow profiles, dynamically following ramping up

Test rig and conditioning

Some picture impression

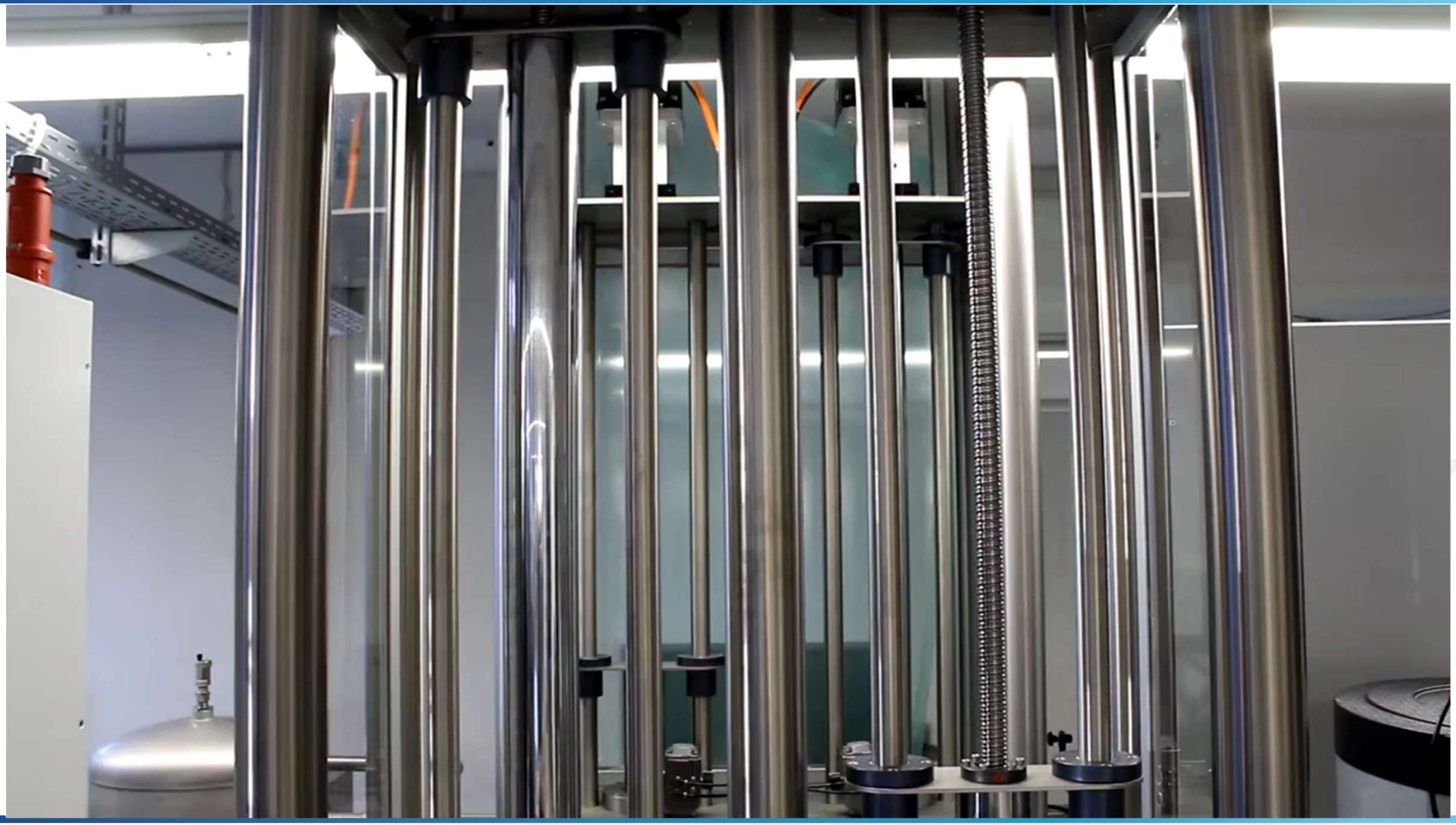

EMATEM

SP (signal processing) / DAQ (data acquisition) / DP (data processing)

- The piston prover provides high-resolution data on the piston position (i.e., volume sections) and the associated time sampling.
- These are synchronously registered each time a pulse appears from the direct output of the sensor (without any treatment).
- The starting point is a certain pulse value [l/p] or a certain encoder constant PC [p/l].
- Ramping up / down; a metrological curve is created in the following way:
- Horizontal X-axis: the instantaneous flow = $(V_{i+1}-V_i)/(t_{i+1}-t_i)*3600$ [l/h]
- Vertical Y-axis: Deviation = $((1\ pulse)/(V_{i+1}-V_i)/PC-1)*100$ [%]
- The medium temperature in the following example = 21.0°C
- The absolute pressure in the system is 5 bar

	A	B	C	D	E	F	G	H	I	J	K	L	M	N	O	P	Q	R	S	T
1	Column1	Column2	Column3	Column4	Column5	Column6	Column7	Column8	Column9	Column10	Column11	Column12	Column13	Column14	Column15	Column16	Column17	Column18	Column19	Column20
2	Zeitsondierung [s] 0	253591.7778	253592.3453	253593.2826	253594.3962	253595.5641	253596.7636	253597.9617	253599.1433	253600.2943	253601.4422	253602.5968	253603.7362	253604.8716	253606.008	253607.131	253608.2273	253609.3192	253610.4226	253611.5079
3	Vol Kolbenauslesung [l] 0	0	0.001443	0.003933	0.006907	0.010049	0.013286	0.016533	0.019764	0.022922	0.026092	0.029301	0.032481	0.035673	0.038876	0.042068	0.045193	0.048329	0.05151	0.054652
4	Zeitsondierung [s] 0	254086.4457	254086.6275	254086.7435	254086.847	254086.9492	254087.0505	254087.1541	254087.2603	254087.3674	254087.4745	254087.5825	254087.6922	254087.7998	254087.9104	254088.0211	254088.1313	254088.2402	254088.3504	254088.4615
5	Vol Kolbenauslesung [l] 0	0	0.004156	0.007203	0.009915	0.012611	0.015274	0.018004	0.020789	0.023585	0.026393	0.029228	0.032108	0.034916	0.037887	0.040703	0.043589	0.04643	0.049304	0.052206
6	Mittlere Impulswertigkeit [l/p]																			
7	0.02058				Aufsteigend	relative Messabweichung		-19.66%	-3.97%	4.37%	7.67%	8.81%	9.00%	8.78%	8.57%	8.38%	8.22%	8.05%	7.92%	7.73%
8	qp1.5 (HS)					Durchfluss [l/h]		0.00	9.66	9.73	9.78	9.83	9.88	9.94	10.00	10.05	10.11	10.16	10.22	10.27
9					Absteigend	relative Messabweichung		-12.52%	1.02%	-5.59%	-6.75%	-6.16%	-5.26%	-4.56%	-3.78%	-3.24%	-2.80%	-2.64%	-2.45%	-2.34%
10	Temperatur [°C] 23.0	Density [kg/m3	997.93			Durchfluss [l/h]		0.00	91.88	94.53	94.50	94.53	94.46	94.37	94.25	94.23	94.27	94.21	94.12	94.06
11	Druck [bar] 5.0	kin visc [m2/s]	9.09E-07			RE Auf		0	157	158	158	159	160	161	162	163	164	165	166	166
12	Rohr InnenD 24.0					RE Ab		0	1489	1532	1531	1532	1531	1529	1527	1527	1528	1527	1525	1524
13	Kapselzähler transparent ohne Zählwerk mit 7 Flügeln																			

Example flow calculation ➔ horizontal axis : right blue flashes group
Example deviation calculation ➔ vertical axis : left blue flashes group

The calculation uses the corresponding blade position in relation to the consecutive rotation position of this particular blade. In other words: “blade-fidelity”. In this example above there are seven blades. In the following cases here there is only one blade.

The degree of approximation of a calculation between different blades would depend on the mechanical design quality of the equiangular blade positions of the rotor.

Remember Ematem-2022: turbine single jet against flow [l/h]; 7 blades; logarithmic

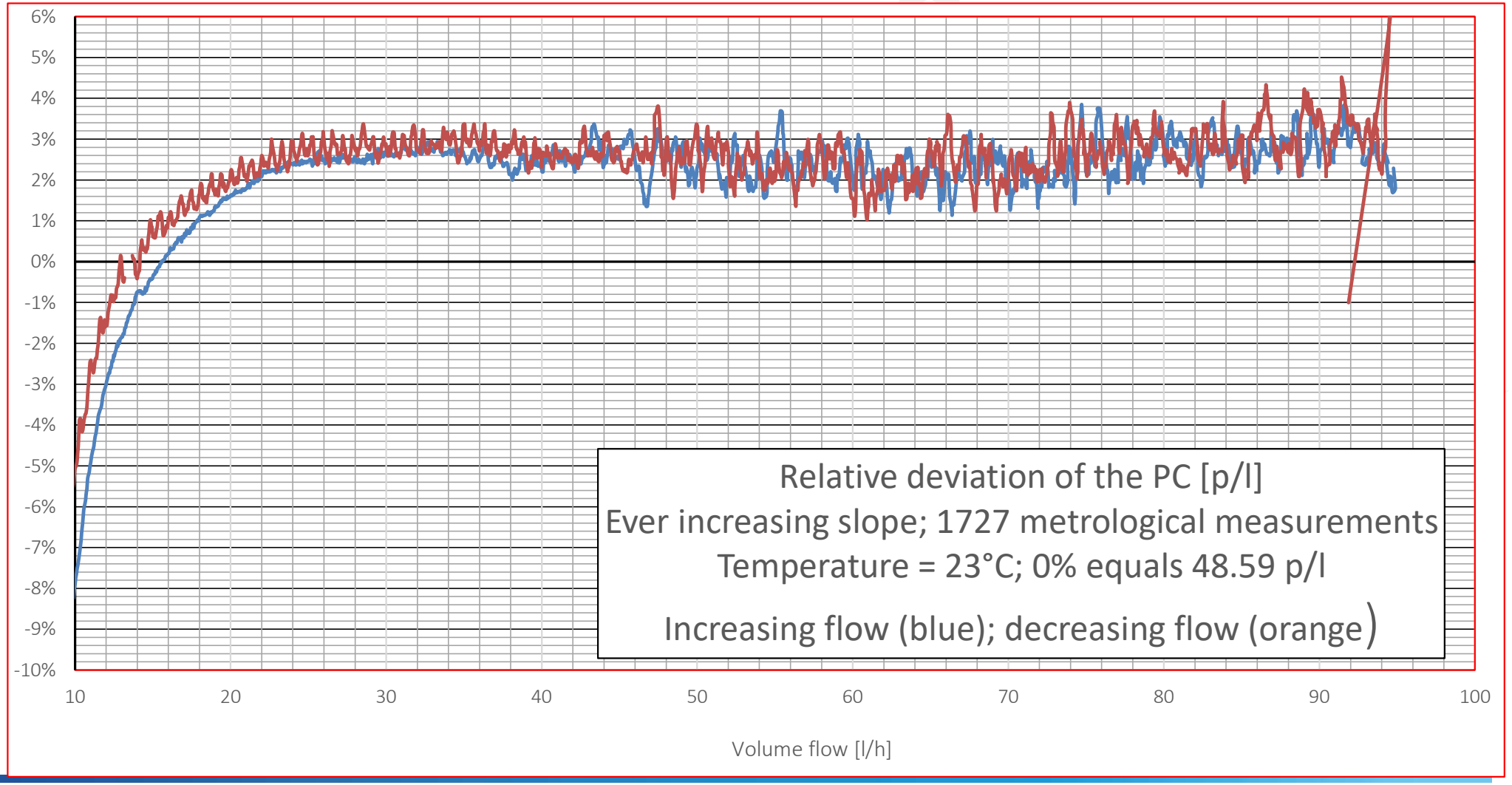

Measurement curve turbine single jet against flow [l/h]; one blade, logarithmic

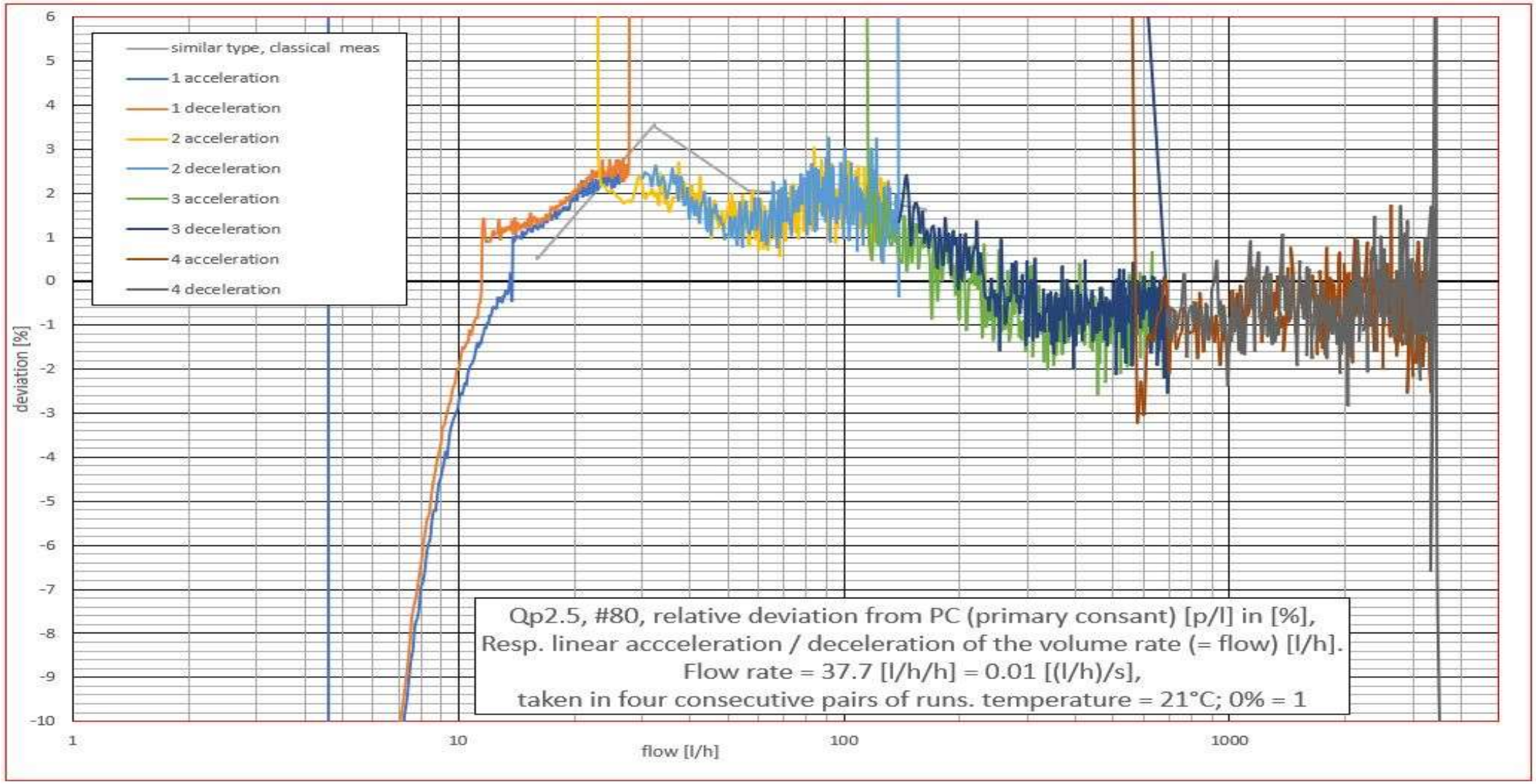

EMATEM

Measurement curve turbine single jet vs Reynolds number [-]; logarithmic

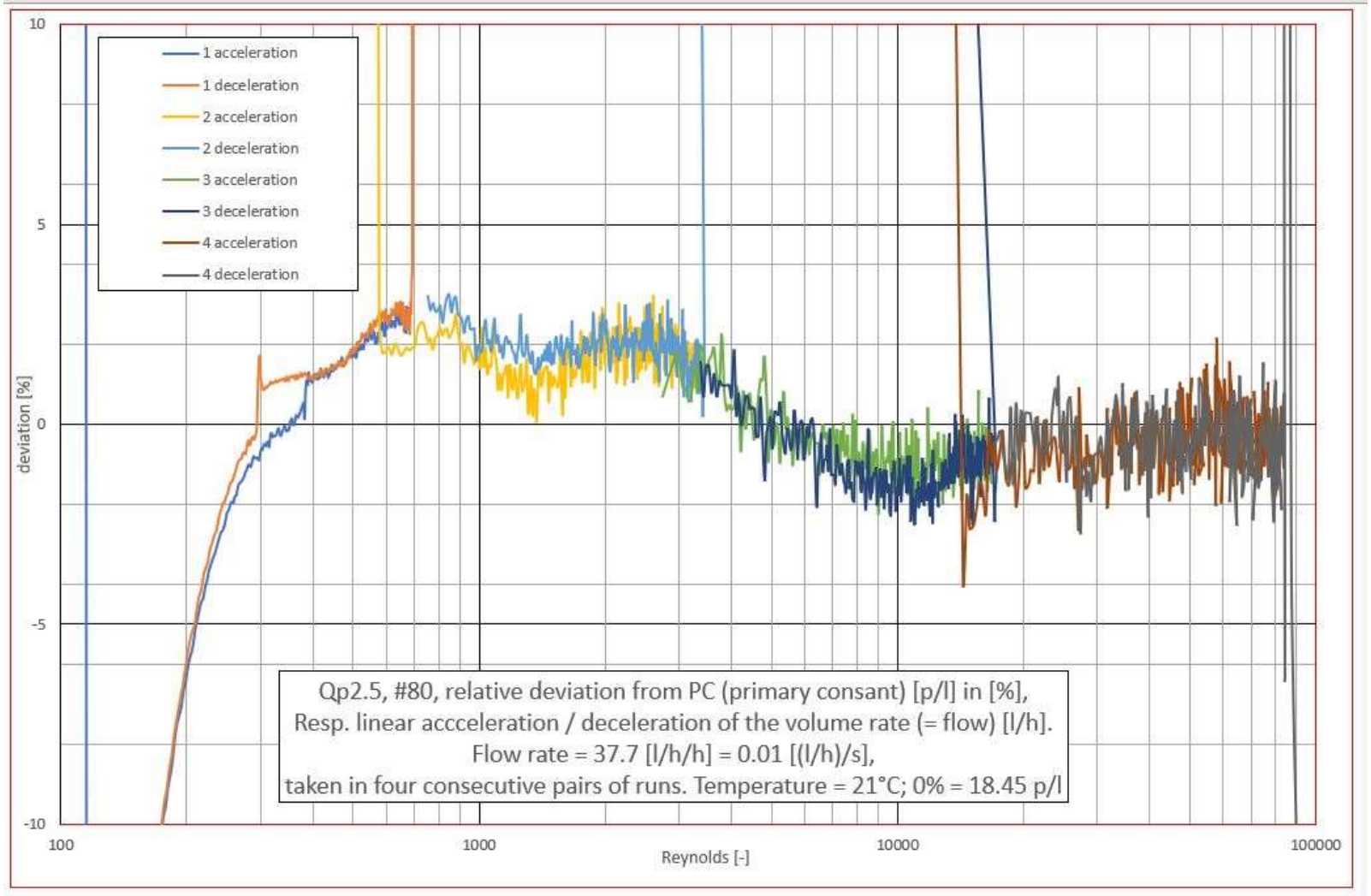

Flow regimes

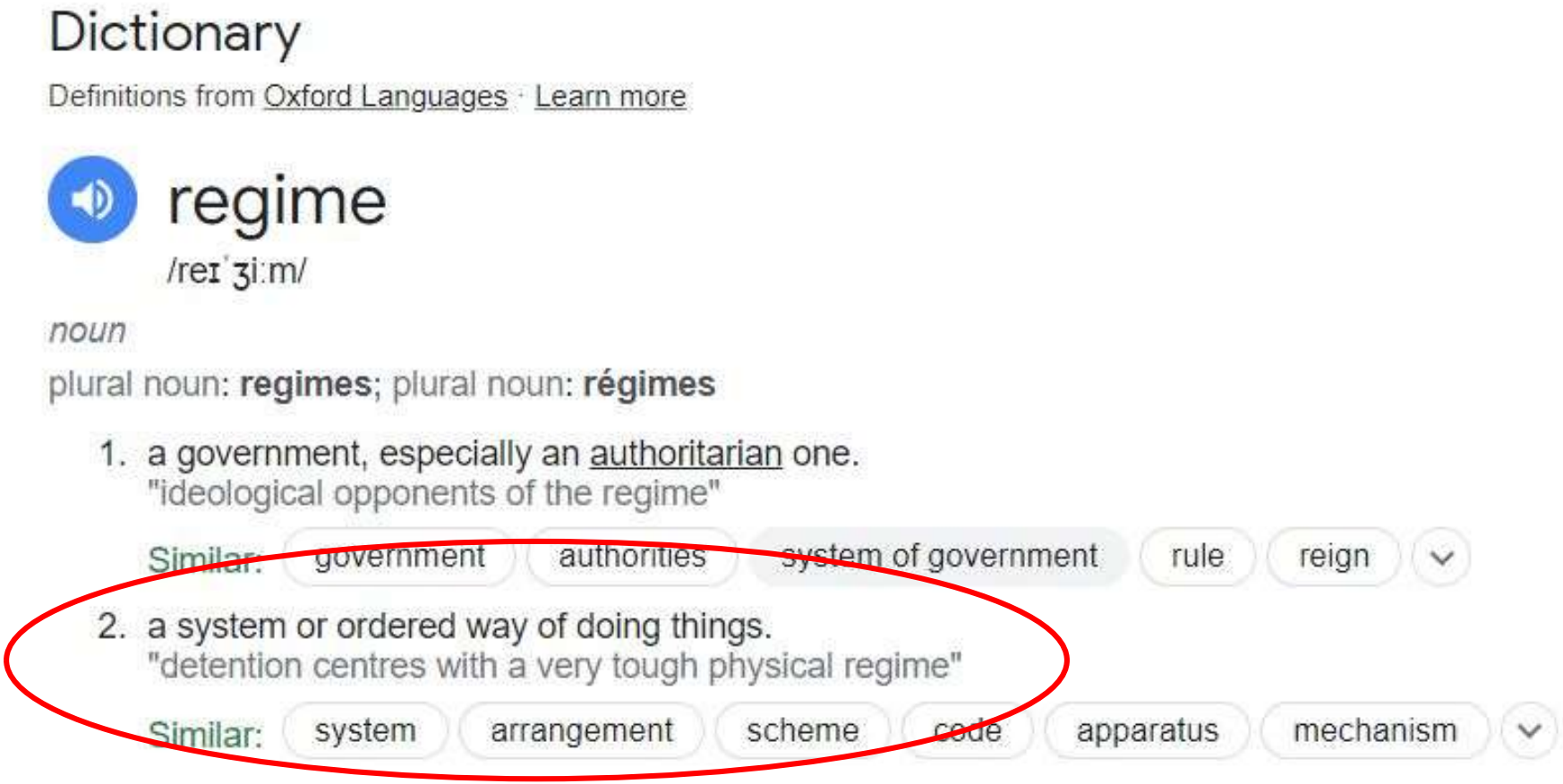

Dictionary

Definitions from Oxford Languages · Learn more

regime

/reɪˈʒiːm/

noun

plural noun: **regimes**; plural noun: **régimes**

1. a government, especially an authoritarian one.
   "ideological opponents of the regime"

   Similar: government | authorities | system of government | rule | reign

2. a system or ordered way of doing things.
   "detention centres with a very tough physical regime"

   Similar: system | arrangement | scheme | code | apparatus | mechanism

Flow regimes

Several turbulent regimes

What are the different flow regimes?

There are three fluid flow regimes: laminar, turbulent, and a transition region. The conditions that lead to each type of flow behavior are system-specific. Fluid flow simulations for various Reynolds numbers can be used to clearly identify and quantify when flow will transition from laminar to turbulent.

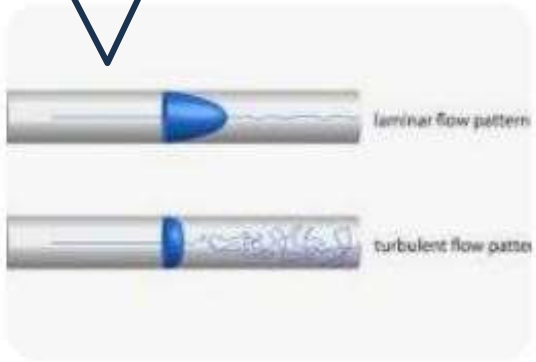

What is a turbulent regime?

Turbulent flow regimes are marked by various fluid current changes or eddies, which vary in size as well as direction. Turbulence also differs from laminar flow in that the Reynolds number is significantly higher, as illustrated in the figure above.

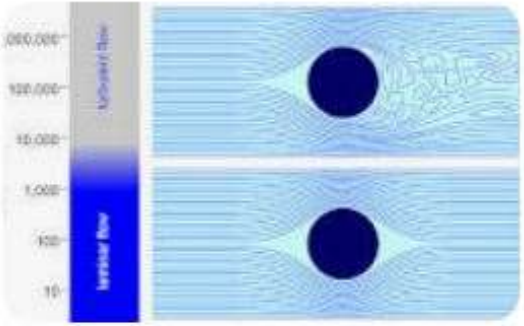

Turbulence is not just turbulence!
Turbulent regimes change with increasing Reynolds numbers, and so their implementation in the Navier-Stokes equations, and so their solutions do.

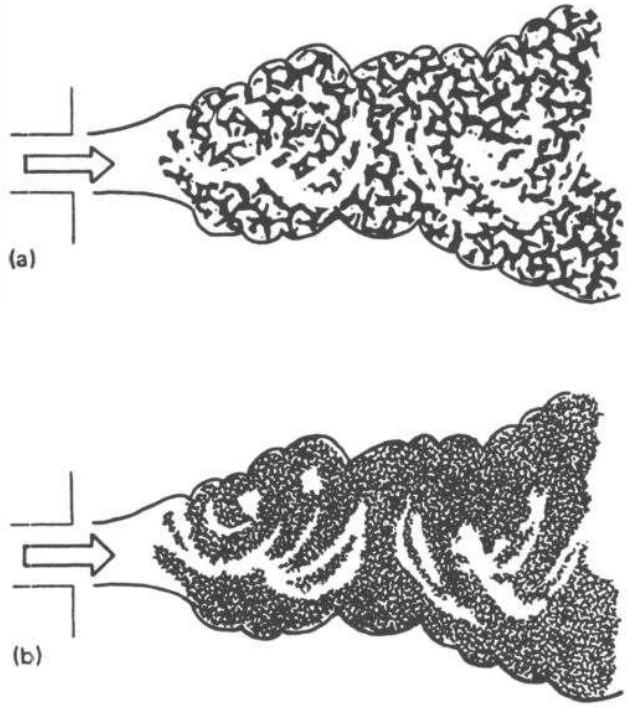

Figure 1.6. Turbulent jets at different Reynolds numbers: (a) relatively low Reynolds number, (b) relatively high Reynolds number (adapted from a film sequence by R. W. Stewart, 1969). The shading pattern used closely resembles the small-scale structure of turbulence seen in shadowgraph pictures.

Examples left side:

A free turbulent jet with relative low - and with higher Reynolds number.

Reference:

A first course in turbulence;

Tennekes and Lumney, MIT press, 1972

Turbulence models describing different flow regimes

What are different types of turbulence model?

The following is a brief overview of commonly employed models in modern engineering applications.

- Spalart–Allmaras (S–A) ...
- k–ε (k–epsilon) ...
- k–ω (k–omega) ...
- SST (Menter's Shear Stress Transport) ...
- Reynolds stress equation model.

What are the methods of turbulence modeling?

Turbulence can be modeled using a variety of approaches, including direct numerical simulation (DNS), large eddy simulation (LES), and Reynolds-averaged Navier-Stokes (RANS) modeling.

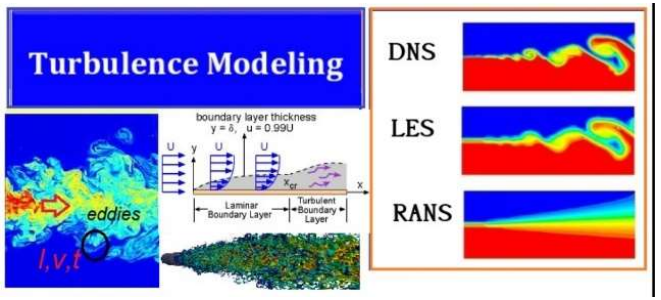

In CFD-simulations often various turbulence models are complementary used, in combination locally adapted to solve the complexity of local structures more adequate.

Transition - Intermittent flow regime

What is the transition model of turbulence?

The transition model calculated an intermittency factor that creates (or extinguishes) turbulence by slowly introducing turbulent production at the laminar-to-turbulent transition location.

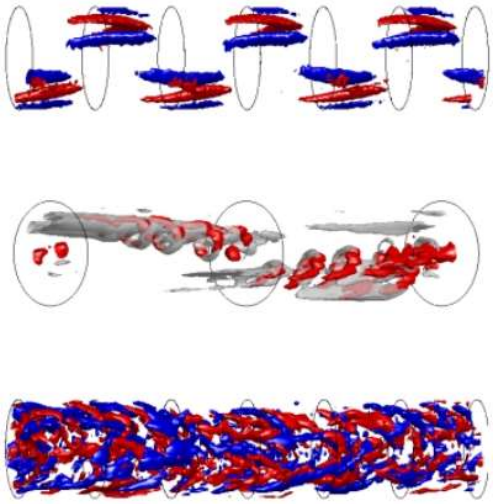

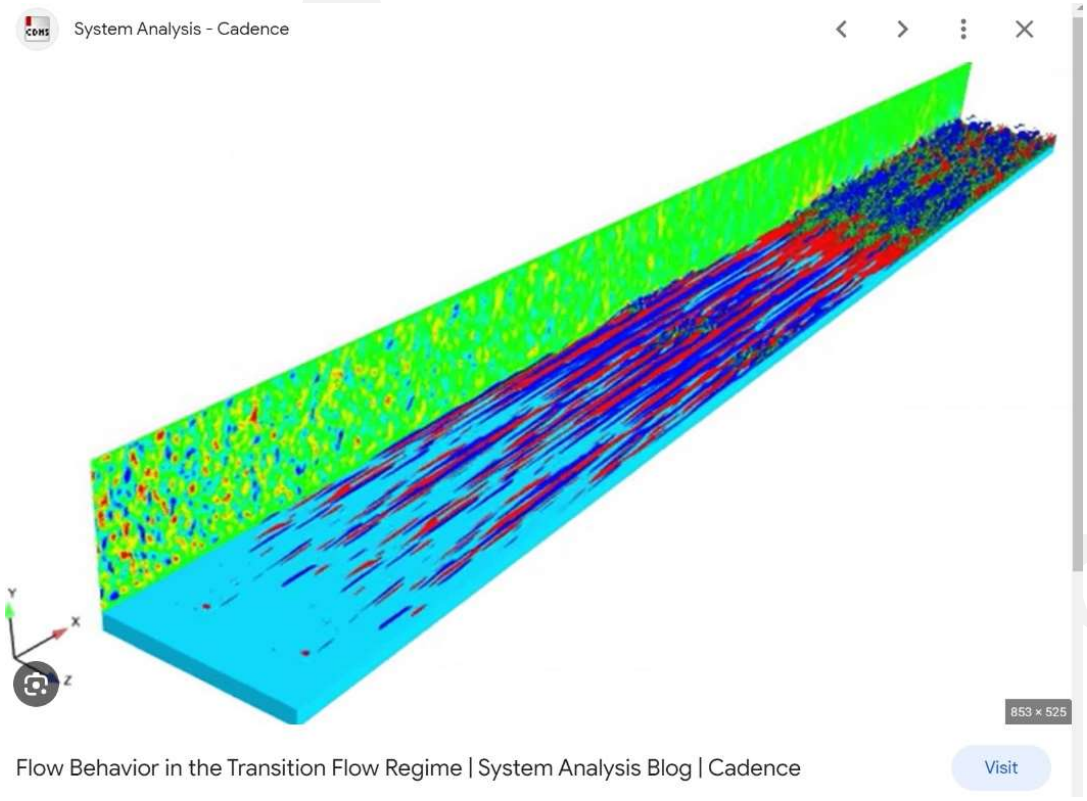

Progressive insights form the last three decades tends to some hysteresis-like alternating dynamic behaviour, rather than one static stable situation; the flow is too high for laminar, so it turns to turbulent, however, it is to slow for turbulent, so it changes to laminar, and so on.

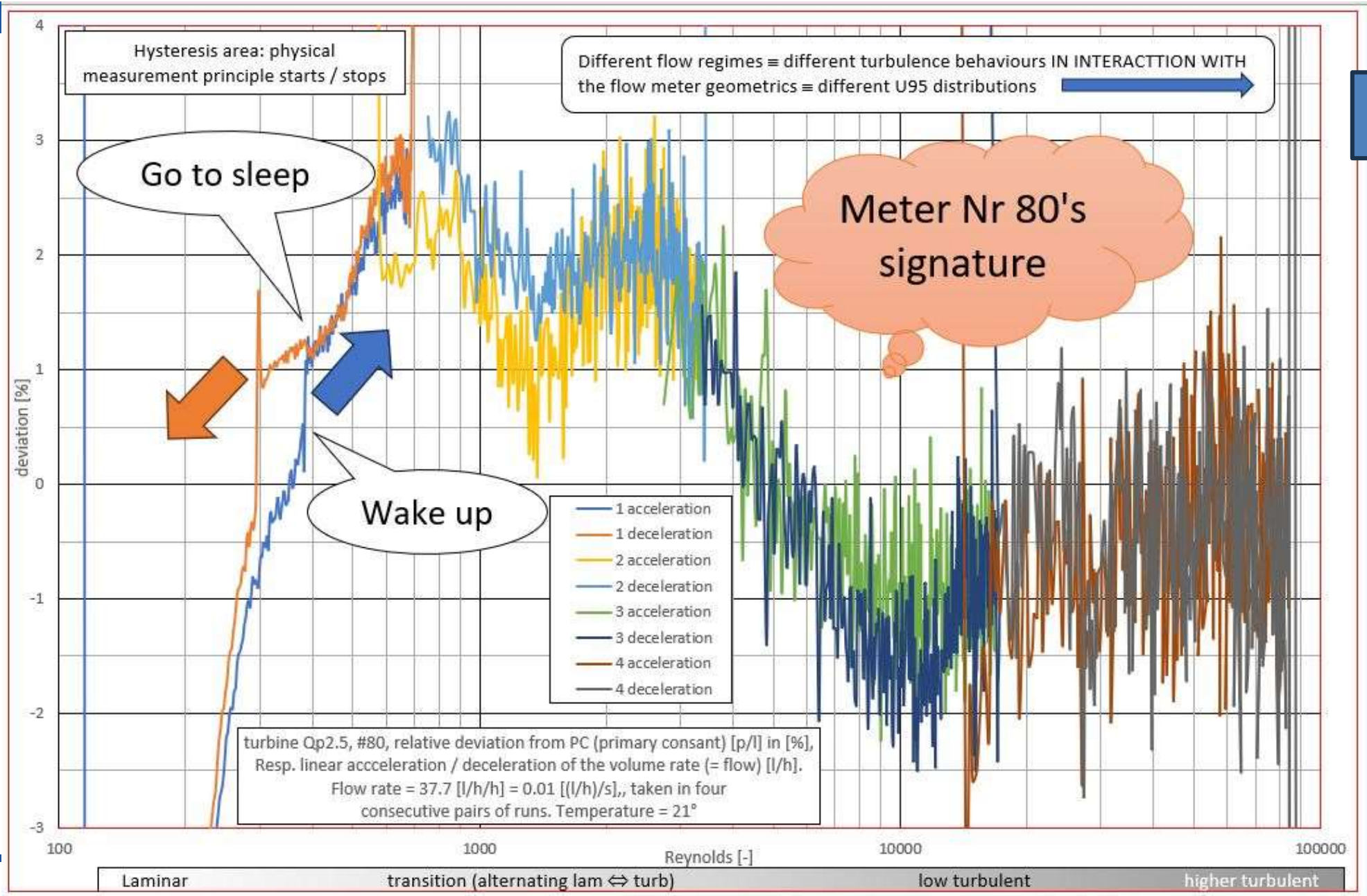
Hysteresis area: physical measurement principle starts / stops
Different flow regimes ≡ different turbulence behaviours IN INTERACTTION WITH the flow meter geometrics ≡ different U95 distributions
Go to sleep
Wake up
Meter Nr 80's signature
deviation [%]
4
3
2
1
0
-1
-2
-3
1 acceleration
1 deceleration
2 acceleration
2 deceleration
3 acceleration
3 deceleration
4 acceleration
4 deceleration
turbine Qp2.5, #80, relative deviation from PC (primary consant) [p/l] in [%], Resp. linear accceleration / deceleration of the volume rate (= flow) [l/h]. Flow rate = 37.7 [l/h/h] = 0.01 [(l/h)/s],, taken in four consecutive pairs of runs. Temperature = 21°
100
1000
10000
100000
Reynolds [-]
Laminar
transition (alternating lam ⇔ turb)
low turbulent
higher turbulent

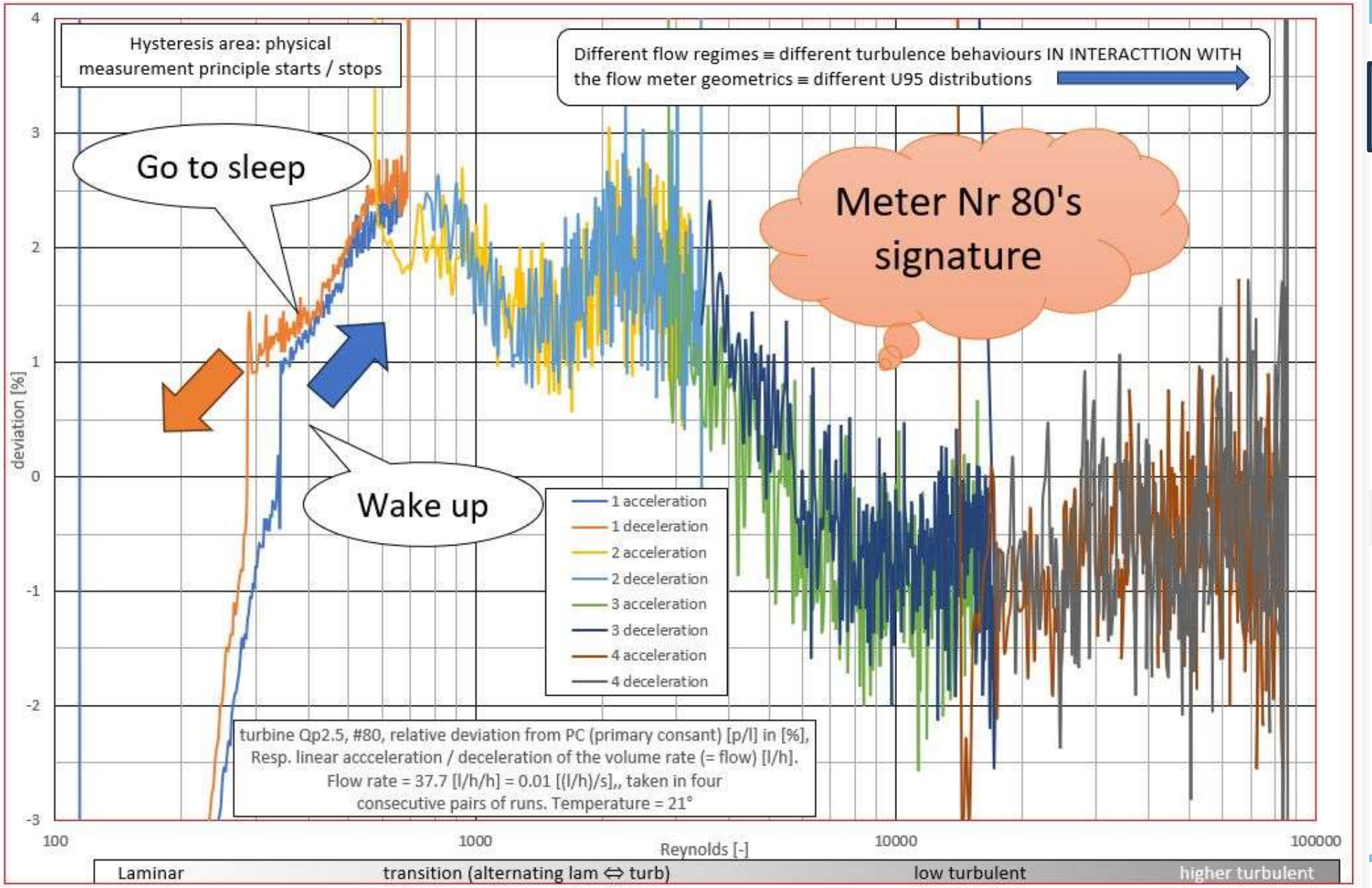
Hysteresis area: physical measurement principle starts / stops
Different flow regimes ≡ different turbulence behaviours IN INTERACTTION WITH the flow meter geometrics ≡ different U95 distributions
Go to sleep
Wake up
Meter Nr 80's signature
1 acceleration
1 deceleration
2 acceleration
2 deceleration
3 acceleration
3 deceleration
4 acceleration
4 deceleration
turbine Qp2.5, #80, relative deviation from PC (primary consant) [p/l] in [%], Resp. linear accceleration / deceleration of the volume rate (= flow) [l/h]. Flow rate = 37.7 [l/h/h] = 0.01 [(l/h)/s],, taken in four consecutive pairs of runs. Temperature = 21°
deviation [%]
4
3
2
1
0
-1
-2
-3
100
1000
10000
100000
Reynolds [-]
Laminar
transition (alternating lam ⇔ turb)
low turbulent
higher turbulent

Regimes spectra

The measured up- resp. down ramping flow domains show the following standard deviations:
There is a significant change between the domains visible.
However, the chosen domains do not correspond with different flow regimes.
---+++---
After Reynolds-reorganisation of the data according to the graph the following table can be found.

NOTE-1: The Reynolds number graph represents the interaction between flow **and** DUT; i.e., the ideal fully-developed flow conditions in undisturbed tube flow (transition: 2000 < Re < 4000) are not present within the DUT. Spectral domain: $U_o=H(s).U_i$ and in time domain: $u_o(t)=h(t)\otimes u_i(t)$, a convolution (Faltung).

NOTE-2: Due to this interaction it is also possible that the now appearing turbulence regimes are split-up in a different way as they would be expected in undisturbed fully-developed tube flow.

	stdev	average up/dwn
1	1.75	
1	1.36	1.55
2	0.46	
2	0.69	0.58
3	0.38	
3	0.21	0.30
4	0.67	
4	0.84	0.76

#80 (2nd)	Re >	Re<	StDev
start-up	1	300	n.a.
laminar	350 (300)	700	0.09
transition	700	1’200	0.07
turbulent-1	1’200	3’500	0.09
turbulent-2	3’500	8’000	0.16
turbulent-3	8’000	18’000	0.10
turbulent-4	18’000	60’000	0.12
turbulent-5	60’000	80’000	0.15

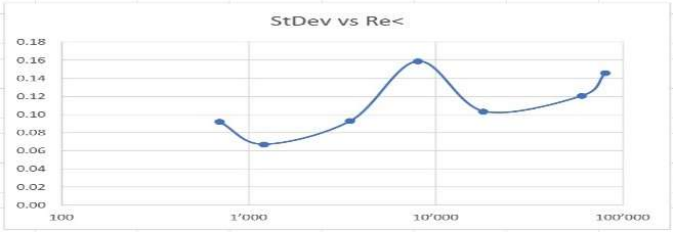

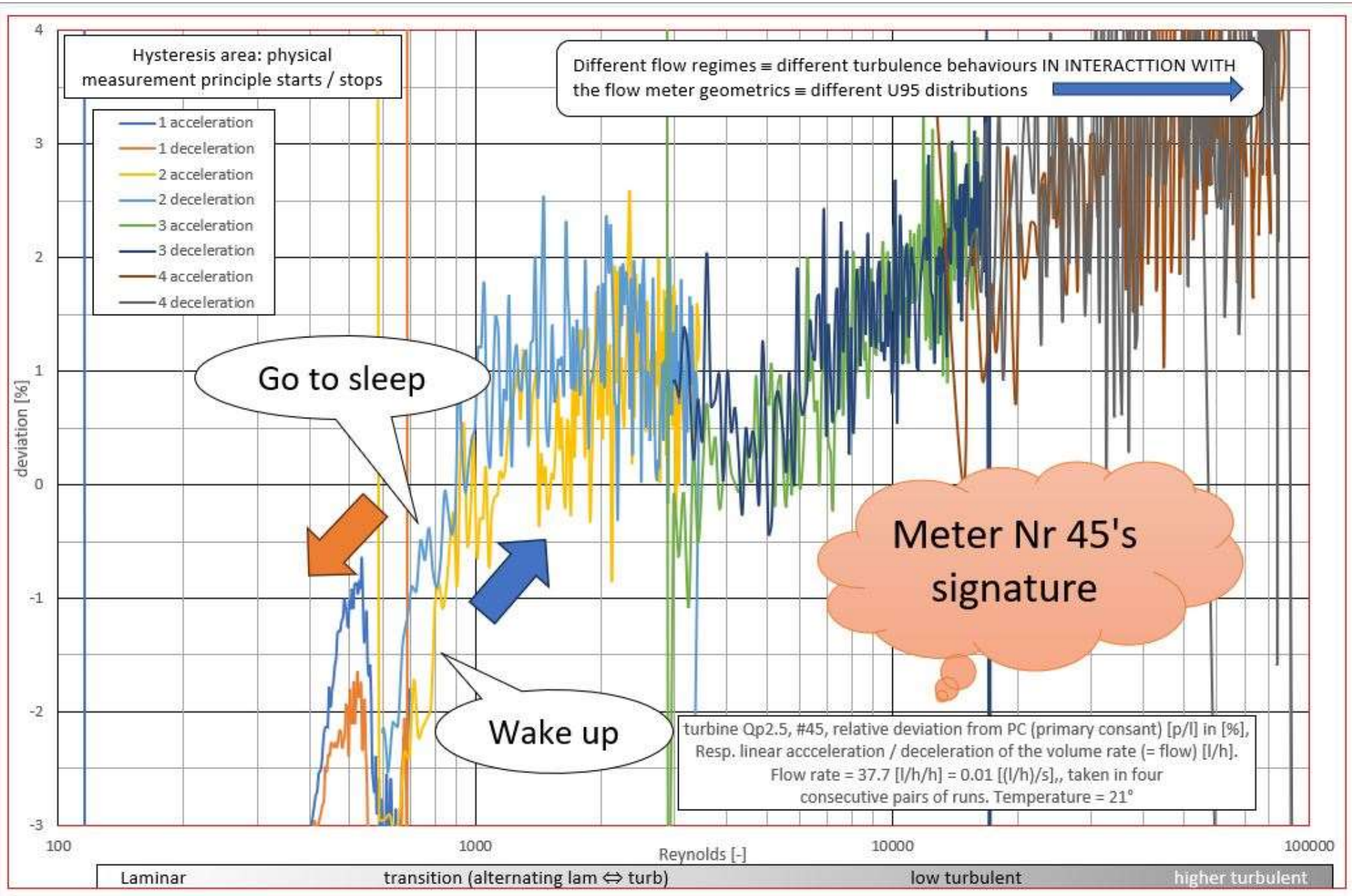

1rst other meter other slope

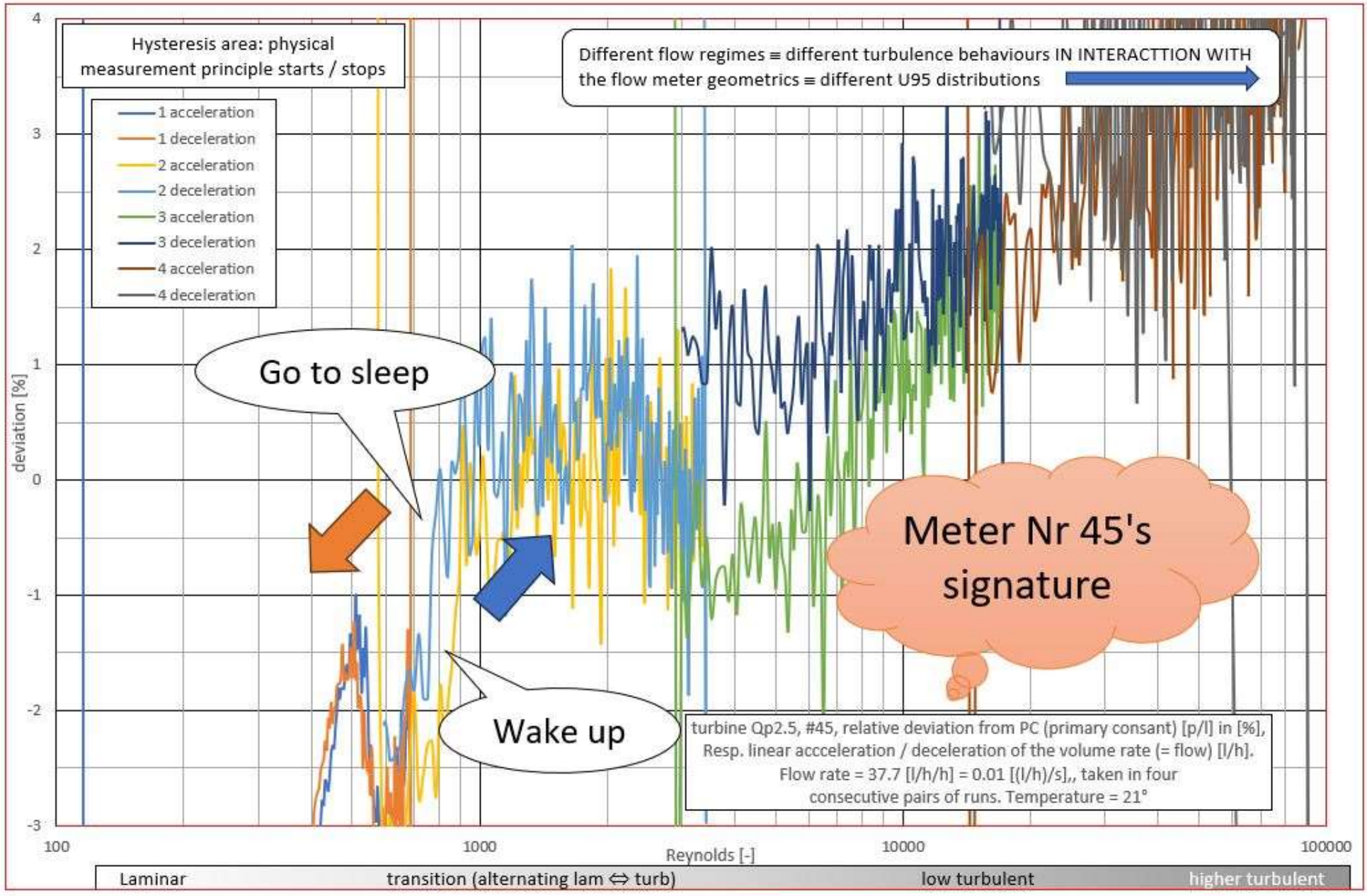

2nd other meter other slope

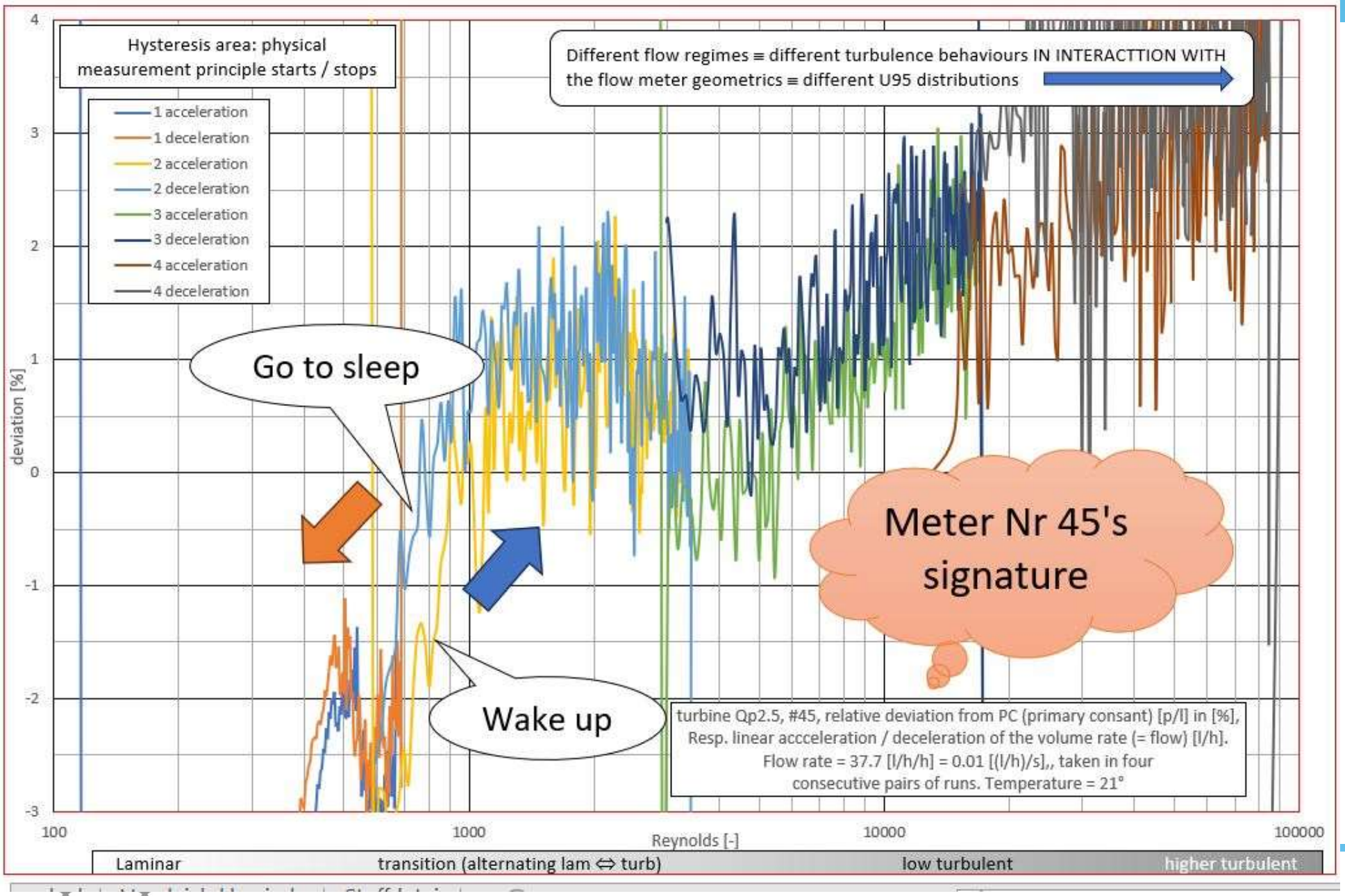

3rd other meter other slope

Spectral interpretation (example glued piezo disk)

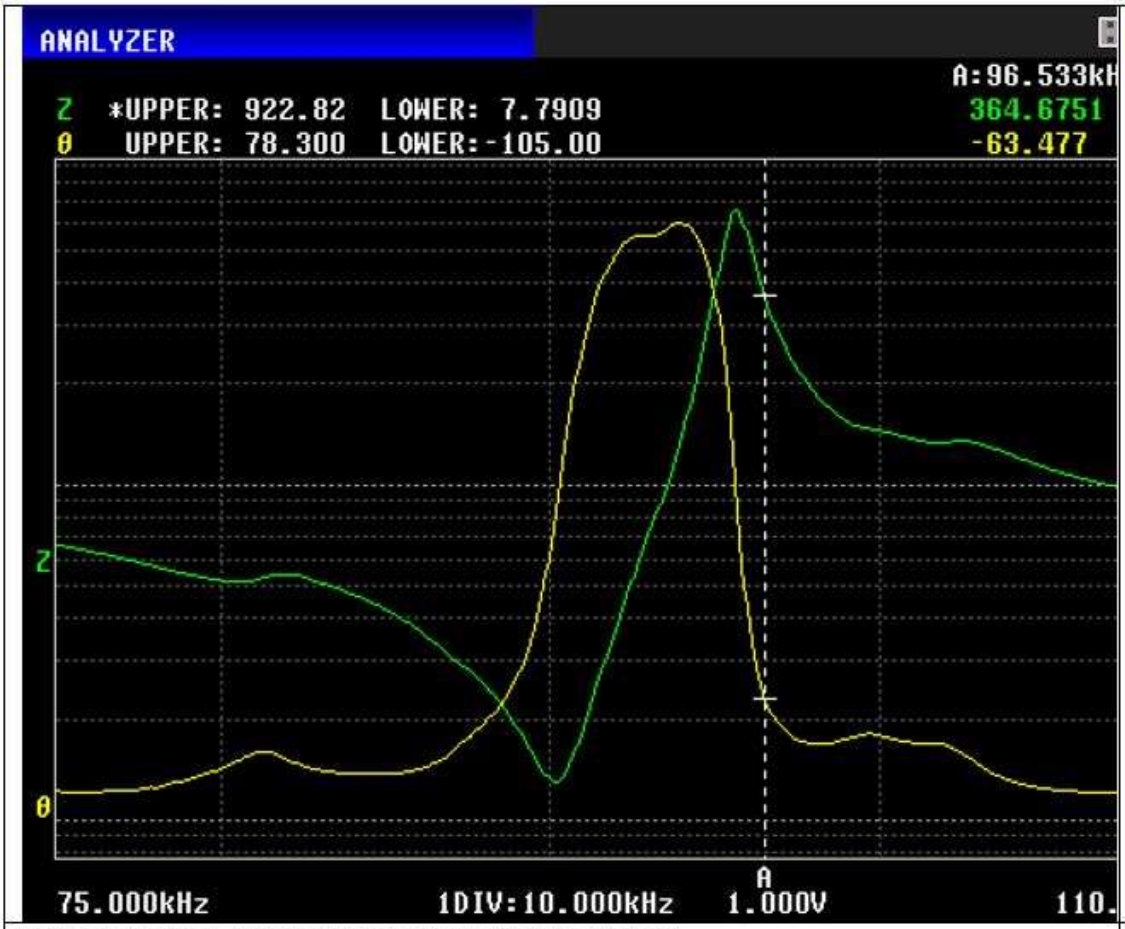

Reference piezo disk: modulus green / phase yellow

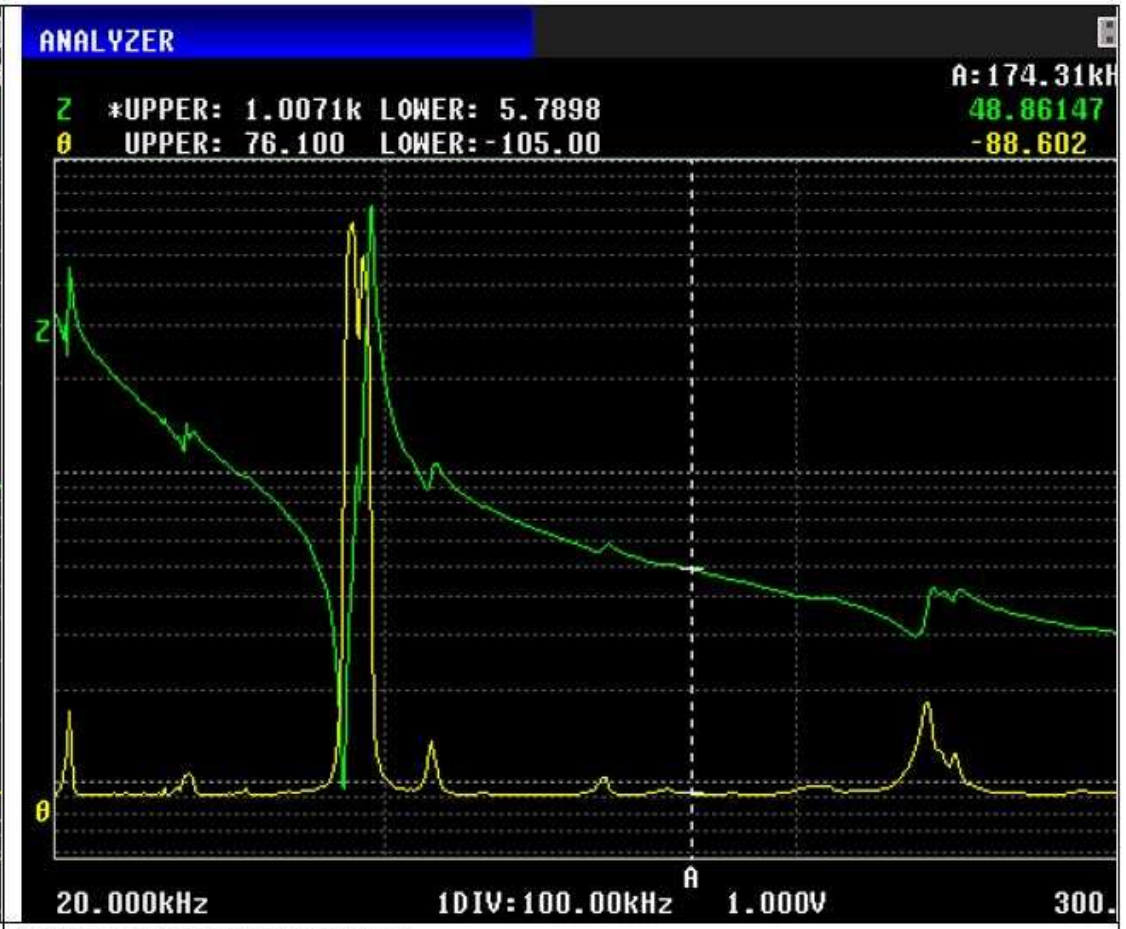

Same, enlarged spectrum view

Spectral interpretation (example glued piezo disk)

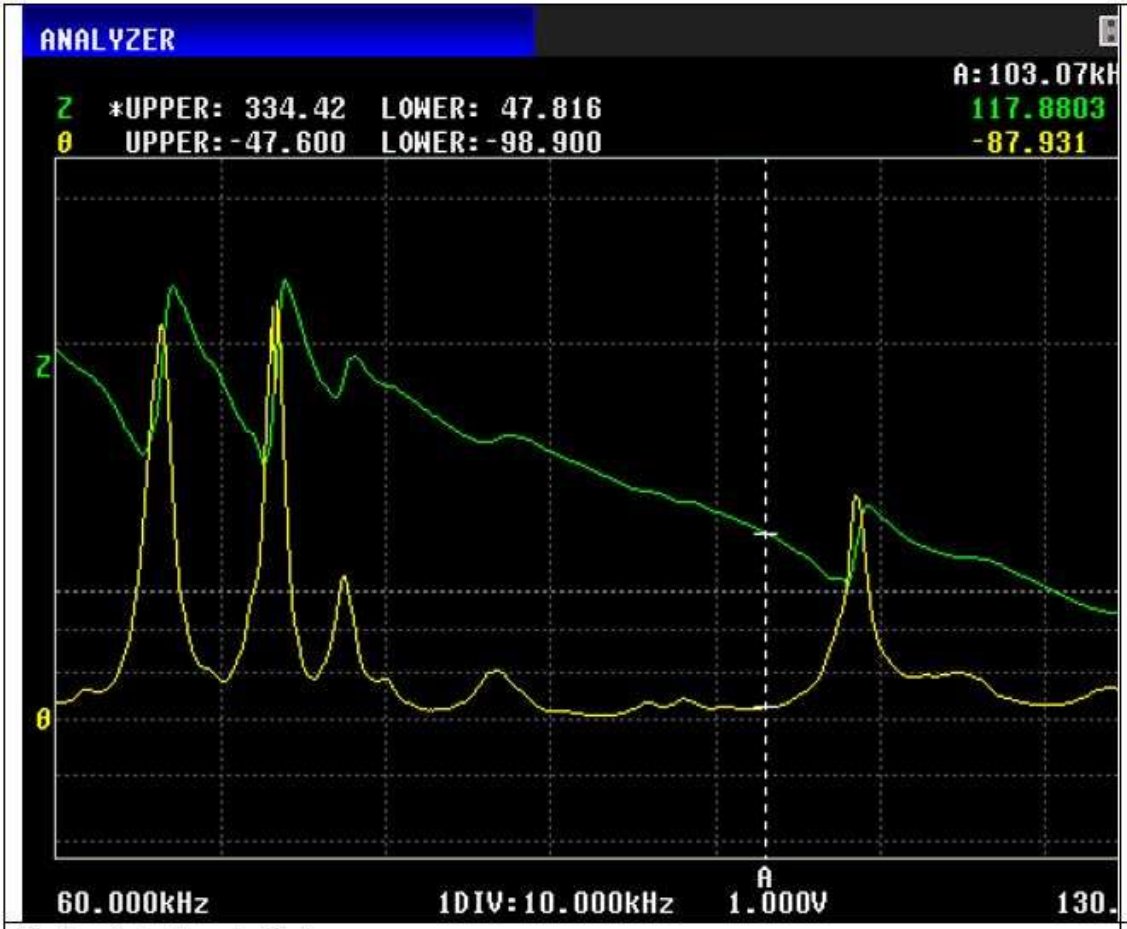

Broken into two half pieces

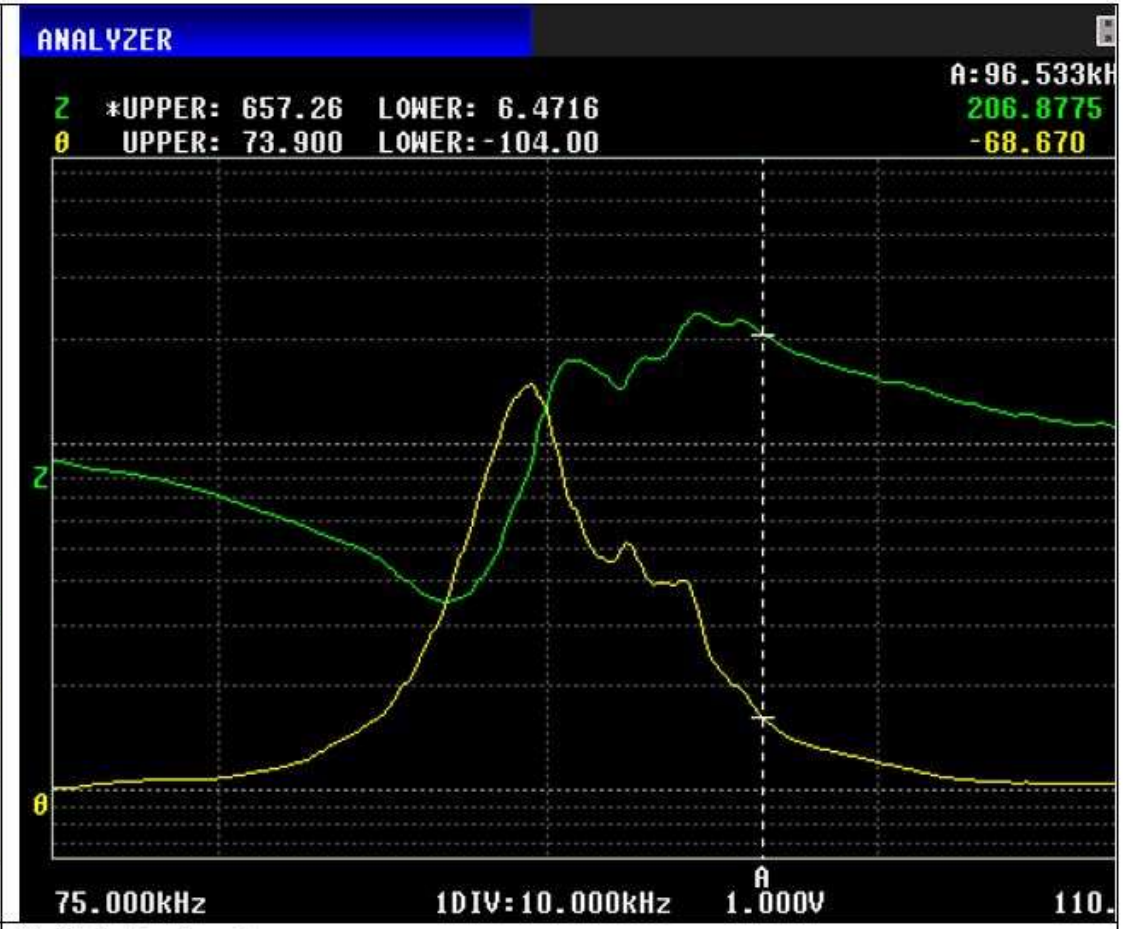

Multiple fractured

Spectral interpretation (example glued piezo disk)

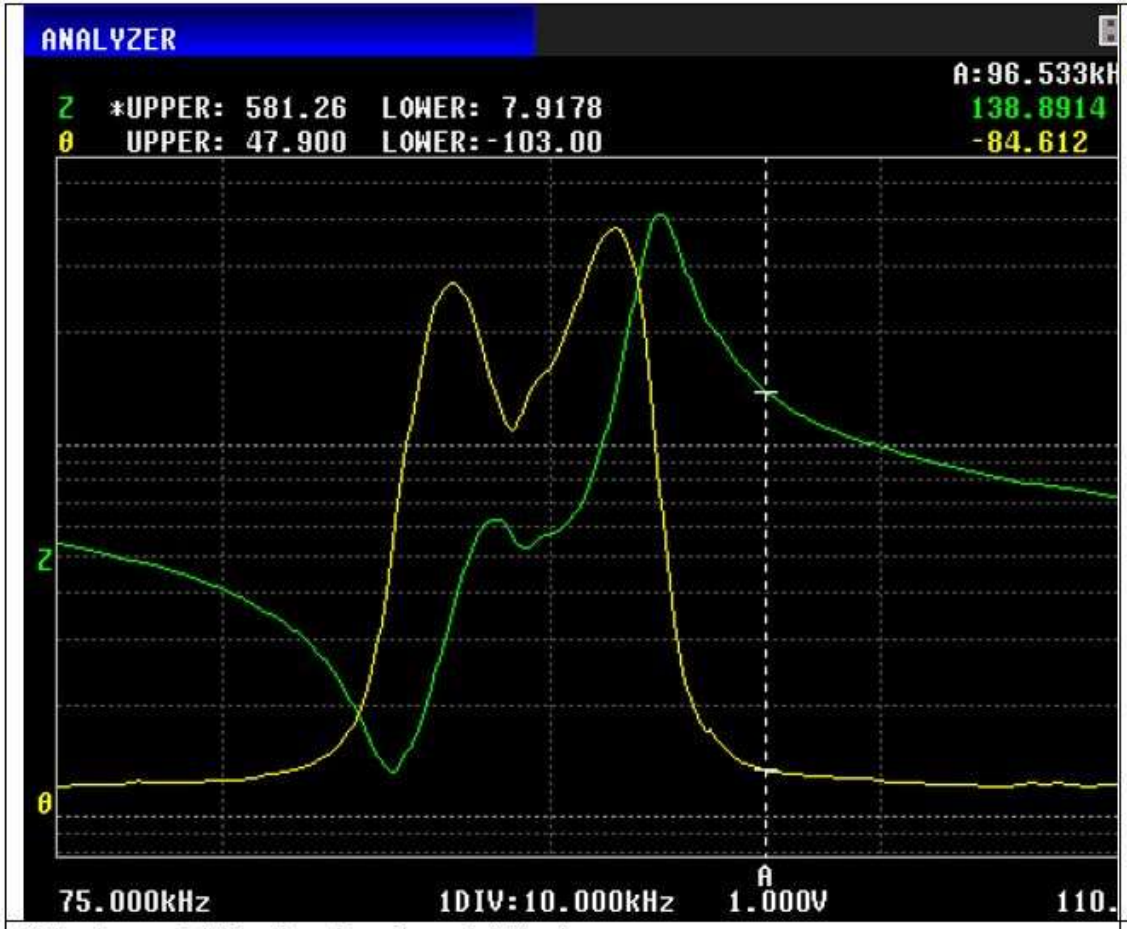

Side clamped (vibrational mode restriction)

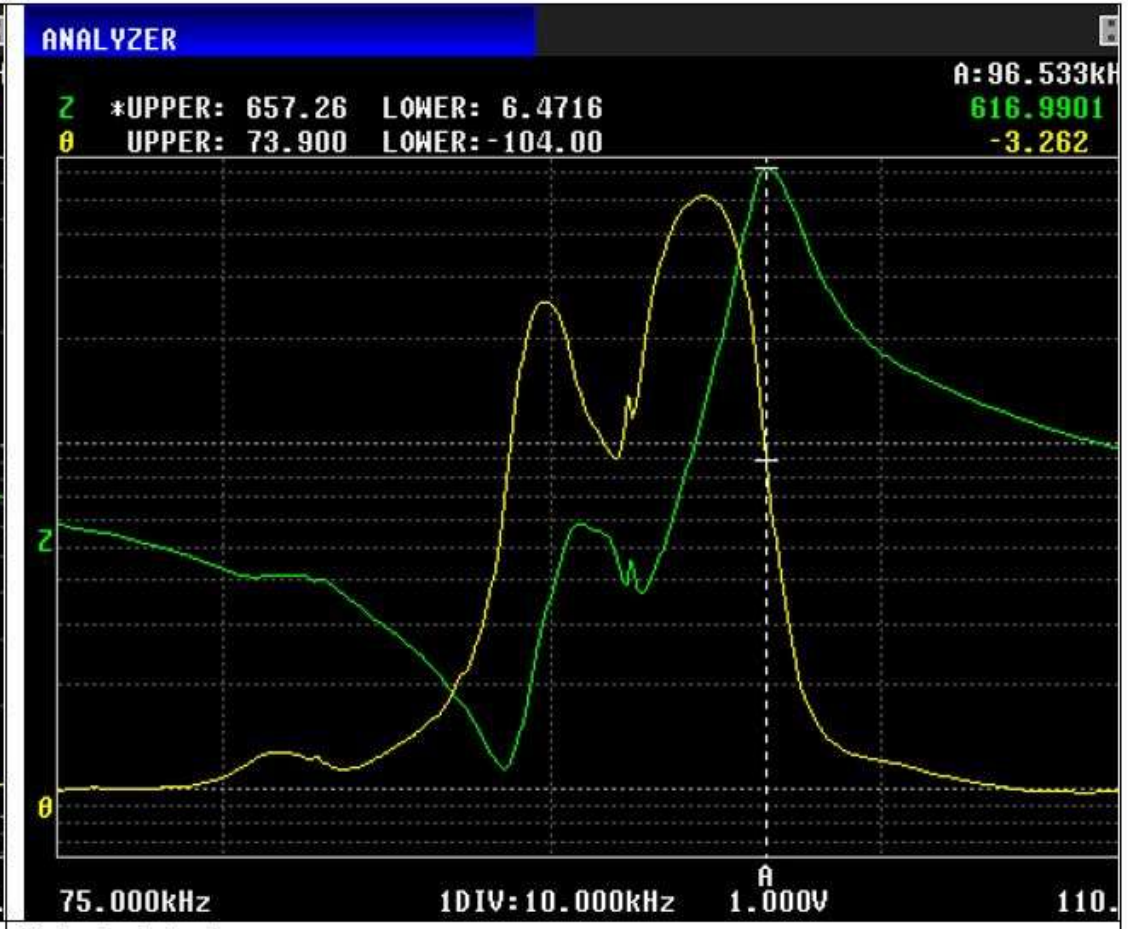

Detached glue layer

Discussion Conclusions Recommendation Consecutive

- data quality
- Redundancy of the Rombach measurements
- measurement of ultrasonic flow meters: $\Delta V/\Delta t$ replaced by ΔTOF
- pulse / step response: inertia hydrodynamic processes involved too slow
- reference measurements on classical rigs as comparison
- meters with defects $\Leftrightarrow$ specific spectral (e.g., sharp edges) characterizing (similar to spectral analyses to piezo-electric disk micro-cracks)
- prediction of the remaining life-time of a meter (similar to airplane spectral turbine surveillance during flights)
- both modulus (Bode) and phase diagrams give related, complementary information, but … how ?

- Traceability (under construction)
- Interpretation encountered phenomena (under discussion)
- The influences of parameter variation (test program)
- Bigger diameters (near future)
- DIN TC176 WG2, EN 1434 consequences, and acceptance

Publication in Nature [2006] by Prof Westerweel TUDelft: “Finite lifetime of turbulence in shear flows”.

Vol 443 7 September 2006 doi:10.1038/nature05089 nature

LETTERS

Finite lifetime of turbulence in shear flows

Björn Hof[1,2], Jerry Westerweel[2], Tobias M. Schneider[3] & Bruno Eckhardt[3]

Generally, the motion of fluids is smooth and laminar at low speeds but becomes highly disordered and turbulent as the velocity increases. The transition from laminar to turbulent flow can involve a sequence of instabilities in which the system realizes progressively more complicated states[1], or it can occur suddenly[2,3]. Once the transition has taken place, it is generally assumed that, under steady conditions, the turbulent state will persist indefinitely. The flow of a fluid down a straight pipe provides a ubiquitous example of a shear flow undergoing a sudden transition from laminar to turbulent motion[4–6]. Extensive calculations[7,8] and experimental studies[9] have shown that, at relatively low flow rates, turbulence in pipes is transient, and is characterized by an exponential distribution of lifetimes. They[8,9] also suggest that for Reynolds numbers exceeding a critical value the lifetime diverges (that is, becomes infinitely large), marking a change from transient to persistent turbulence. Here we present experimental data and numerical calculations covering more than two decades of lifetimes, showing that the lifetime does not in fact diverge but rather increases exponentially with the Reynolds number. This implies that turbulence in pipes is only a transient event (contrary to the commonly accepted view), and that the turbulent and laminar states remain dynamically connected, suggesting avenues for turbulence control[10].

An abrupt transition to turbulence occurs in a large variety of situations, ranging from the formation of spiral galaxies, to the fluid motion in the atmosphere and oceans, to flows over aeroplane wings or through blood vessels. The flow down a circular pipe is a prime example, and an experimentally accessible realization, where such a transition occurs despite the linear stability of the base flow[11]. We have recently developed a description for the onset of turbulence in pipes that focuses on the appearance of unstable travelling waves as the dimensionless flow rate—the Reynolds number, Re—is increased[3,12–14] (here $Re \equiv UD/\nu$, where U is the mean flow speed, D the pipe diameter and ν the kinematic viscosity of the fluid). These new solutions show up transiently in the turbulent signal, and are thought to connect to form a chaotic saddle[15,16]. The most significant evidence for the formation of a chaotic saddle is the observation of the decay of turbulence at some point in time without any noticeable prior indication[8,9,17]. If the probability of decay is constant in time and independent of when the turbulence was started, then the distribution of lifetimes is exponential, as in radioactive decay. Evidence for the presence of a chaotic saddle comes from the observation of such exponential distributions in pipe flow[8,9] and in plane Couette[18,19] flow (the flow of a fluid layer between two moving walls).

Formally, the probability of finding a turbulent flow state at a time t as a function of the Reynolds number can be expressed as:

$$P(t, \mathrm{Re}) = \exp[-(t - t_0)/\tau(\mathrm{Re})] \quad (1)$$

where t is the time since the start of the experiment, t_0 a constant delay related to the initial formation of a turbulent flow state ($t_0 \ll \tau$), and τ is the characteristic lifetime, which depends on Re. The very rapid increase of $\tau(\mathrm{Re})$ with Re reported in earlier studies[8,9,18] led to the conclusion that τ diverges at some finite Reynolds number $\mathrm{Re}_{\mathrm{crit}}$, that is, $\tau(\mathrm{Re}) \propto 1/(\mathrm{Re}_{\mathrm{crit}} - \mathrm{Re})$. Such a divergence would imply that the system undergoes a transition from a transient chaotic saddle to a permanent chaotic attractor. Here we will reconsider this conclusion in view of new experimental and numerical results for observation times that span more than two orders of magnitude.

On the experimental side, a 30-m-long pipe was constructed from 20 precision bore copper segments, each 1.5 m long with an internal diameter of $D = 4$ mm (±0.06 mm): this gives a maximal length to diameter ratio of 7,500. The flow was gravity driven, thus allowing an extremely accurate control over the flow rate (better than 0.1%), which is a crucial requirement for lifetime measurements. The friction factor of the laminar flow accurately follows the Hagen-Poiseuille law (see Supplementary Fig. S1, and Supplementary Methods), confirming the quality of the experimental set-up. Turbulent structures (so-called turbulent puffs[20,21]) were created by injecting a water jet for 0.8 s through one of twenty 0.6 mm holes in the pipe wall; these holes were equally spaced along the pipe. The turbulent structure thereby created travels down the pipe at approximately the bulk flow speed[20,22], and the observation time is set by the distance between the chosen perturbation point and the pipe end. The pipe length of $7{,}500D$ allows a maximum observation time of $t = 7{,}500\ D/U$; this is ten times longer than the maximal observation times in the currently longest laboratory pipe facilities, and ten times that reached in numerical calculations. As the small diameter of the pipe makes velocity measurements (such as particle image velocimetry or laser Doppler measurements) difficult, a much simpler but equally effective way of distinguishing laminar from turbulent flow[23] was chosen here. Because the centre-line velocity of turbulent flow is reduced by ~30% with respect to the laminar profile while the velocities close to the wall increase, turbulent and laminar flows leave the pipe at distinctly different angles (Fig. 1). By monitoring the jet leaving the pipe, we can therefore determine if a turbulent puff created upstream has survived the journey downstream.

In previous studies[8,9,18], the probability $P(t,\mathrm{Re})$ was measured at fixed Reynolds numbers as a function of time t. In the present set-up, it was more practical to keep the dimensionless observation time, t/D (that is, the distance between the point of perturbation and the outlet), fixed, and to vary the Reynolds number. From equation (1) and an assumed divergence of the characteristic lifetime, $\tau(\mathrm{Re}) \propto 1/(\mathrm{Re}_{\mathrm{crit}} - \mathrm{Re})$, we would expect that $P(t,\mathrm{Re})$ increases exponentially with Re, that the steepness of the exponential increases with t and that independent of the value of t all curves reach $P = 1$ at $\mathrm{Re}_{\mathrm{crit}}$ (Fig. 2a inset). Clearly, our measurements (Fig. 2a) do not support this

[1]School of Physics and Astronomy, The University of Manchester, Manchester M13 9PL, UK. [2]Laboratory for Aero & Hydrodynamics, Delft University of Technology, 2628 CA Delft, The Netherlands. [3]Fachbereich Physik, Philipps-Universität Marburg, 35032 Marburg, Germany.

expectation. The data fall along S-shaped curves, which bend in the direction of larger Re as P increases towards 1. Moreover, by appropriate shifts in Re, the data for different observation times can be collapsed onto a single curve (Fig. 2b). The shape of this curve clearly does not show the steep rise expected for lifetimes diverging at a finite $\mathrm{Re}_{\mathrm{crit}}$.

The possibility of mapping the observations for different times onto one curve by shifting the Reynolds number suggests an exponential relation between the characteristic time and the Reynolds number, of the form $\tau^{-1} = \exp(a + b\mathrm{Re})$, with constants a and b. (Note that here and in the following all times are presented in their dimensionless form, unless stated otherwise.) This functional dependence implies that the shifts $\Delta\mathrm{Re}$ needed to map the probability distributions for observation times t_1 and t_2 on top of each other are given by $\Delta\mathrm{Re} = (1/b)\ln[(t_1 - t_0)/(t_2 - t_0)]$. This is indeed the case (Fig. 2b inset), and confirms the exponential scaling of τ. Alternatively, $\tau(\mathrm{Re})$ can be obtained directly from the data in Fig. 2a, and these verify the exponential scaling obtained above, as shown in Fig. 3a. From these fits, we obtain a good representation of our data with $b = -0.0344$, $a = 59.28$ and $t_0 = 120$. Substituting these parameters into equation (1) gives the theoretical curves shown in Fig. 2a, which reproduce the S-shape of $P(t,\mathrm{Re})$. In conclusion, the S-shape of the distributions in Fig. 2a, the scaling of shifts required to overlap these curves, the absence of divergence at a critical Reynolds number, as well as the characteristic lifetimes shown in Fig. 3a, are all fully consistent with the exponential scaling proposed for τ^{-1}. Clearly these features cannot be explained by the linear scaling proposed in earlier studies.

Direct numerical simulations of flow in pipes cannot at present reach these long observation times, and are limited by the extent of the numerical domain. Nevertheless, simulations that we performed for a length of $5D$ with periodic boundary conditions and for observation times up to $t = 3{,}000\ RU_{cl}/\nu$ (here R is the pipe radius and U_{cl} the centre-line velocity) agree with the experimental observations, and support the conclusion of transient turbulence with a characteristic lifetime that increases exponentially with Reynolds number (Fig. 3b). In these simulations, the flow was initially disturbed and integrated in time until the turbulent disturbance decayed or the maximum integration time of 3,000 was reached. For every Reynolds number, 100 independent simulation runs were analysed to extract the probability distribution of lifetimes (Supplementary Methods, Fig. S2), and τ^{-1} is again found to vary

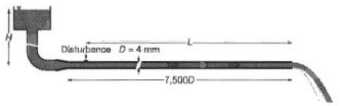

Figure 1 | Sketch of the experimental apparatus. The pipe sections were accurately aligned with a laser, ensuring that deviations were smaller than 2 mm over the entire 30 m length (30 m = $7{,}500D$, where D is the internal diameter, 4 mm). The flow is driven by a constant pressure head (H) and remained laminar up to Reynolds numbers greater than 2,750, where perturbations at the inlet become large enough to trigger turbulence; this is well above the largest Reynolds number of our measurements. During each measurement, a jet is injected into the laminar flow at a distance L from the pipe entrance with the aid of a high-speed solenoid valve. This perturbation creates a turbulent patch of fluid, a so-called turbulent puff. Gravity feeding ensures a constant pressure difference along the pipe, but the flow rate will drop when turbulence sets in, owing to the increased drag. However, all our studies are limited to a regime where the turbulent structures are smaller than $2D$ in length and their size remains constant[13,21]. Theoretical estimates and experimental observations show that the maximum decrease in the flow rate caused by a single turbulent event is smaller than 0.25%. The turbulent puff travels downstream at the mean velocity towards the pipe exit where the turbulent flow (red velocity profile) can be distinguished from the laminar one (blue profiles) by a distinct drop in the outflow angle (shown dashed). The fluid was then pumped back into the header tank, keeping H constant to within 0.1%. The distance between the pipe entrance and the perturbation point could be varied in 20 steps of length $375D$, resulting in an equal change of the observation time, t.

Figure 2 | Lifetime distributions. a, Probability distributions of lifetimes measured experimentally for fixed values of t (time since the start of the experiment) as a function of Reynolds number, Re. Each data point has been obtained from 30 to 75 rehearsals of the experiment. The distributions are S-shaped, flattening when approaching probability $P = 1$. With increasing t, the distribution curves shift to larger Re. The fitted lines are of the form $\exp[-(t - t_0)/\tau]$ with $\tau^{-1} = \exp(a + b\mathrm{Re})$; here t_0 is a constant delay, τ is the characteristic lifetime, and a and b are fitting parameters. The error bars represent the absolute uncertainty in the Reynolds number (for details see Supplementary Methods). Inset, theoretical predictions for a linear scaling of $1/\tau$ with Re. **b,** Same data as in **a** but with the curves collapsed by appropriate shifts $\Delta\mathrm{Re}$ in Reynolds number, confirming that the shape of the distributions does not change notably with increasing t. The fitted line is obtained with the fitting parameters a and b from panel **a**. Inset, the ratio of observation times as a function of $\Delta\mathrm{Re}$. The exponential correlation is in accord with the suggested exponential variation of lifetimes with Re. The straight line is obtained with the fitting parameters a and b from panel **a**.

exponentially with Re (Fig. 3b). The main difference between experiments and the simulation is the finite length of the simulated pipe. Additional simulations of a longer pipe indicate that the same lifetimes are reached at lower Re.

Our observation of non-diverging lifetimes can be shown to be fully consistent with the data of previous studies, where a different conclusion had been drawn: reanalysing the numerical data of ref. 8

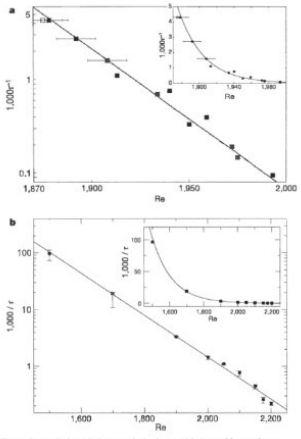

Figure 3 | Variation of characteristic times with Reynolds number. **a,** The reciprocal characteristic lifetimes as a function of Re for all experiments with $t_0 = 120 D/U$. They were obtained from fits to the data shown in Fig. 2a. Each data point required 400 to 500 measurements, with the total number of experiments underlying the figure exceeding 5,000. The straight line is an exponential fit to the data points. Error bars represent absolute errors based on experimental uncertainties (see Supplementary Methods for details) and are representative for all data points. Lifetimes were observed to be independent of the amplitude of the perturbation that initially created the turbulent patch. Typically, the volume flux injected at the perturbation point to trigger turbulence was 0.07 times the volume flux in the pipe. The open symbol presents a set of measurements where turbulent puffs were created by perturbation amplitudes four times larger than for the neighbouring symbol; both measurements agree within the experimental uncertainties. Inset, the same data replotted on a linear scale, underlining that they are not compatible with a divergent characteristic lifetime (error bars are the same as in the main figure). **b,** Characteristic lifetimes obtained from numerical simulations of pipe flow. The values of τ have been extracted from the slopes of the exponential tails of the probability density function, PDF, of lifetimes (see also material shown in Supplementary Fig. S2), and are plotted as a function of Re on a logarithmic scale and on a linear scale (inset). The curves correspond to an exponential fit to the data. The data clearly support an exponential scaling of τ as a function of the Re. The error bars represent the statistical uncertainties of the exponential fits. More precisely they show the range of values compatible with the calculated PDF.

by taking a non-zero t_0 into account reveals that lifetimes indeed vary exponentially with Reynolds number. Concerning the experimental lifetime measurements[9], it is apparent from Fig. 3a inset that an exponential scaling of τ^{-1} can only be distinguished from a linear one if observation times exceed $t = 1{,}500$; this is much longer than the 500 available in ref. 9. Turning to other systems, evidence for a non-diverging lifetime can be found in calculations for Couette flow[24], where $P(t,\mathrm{Re})$ also shows the characteristic S-shaped form (see Supplementary Methods, Fig. S4). Similarly, the experimental data for plane Couette flow[18] (see Supplementary Methods, Fig. S3) also show an exponential variation of the characteristic lifetimes once t_0 is taken into account. Finally, we mention that exponential behaviour is also found in a shear flow model[25].

We have shown that in contrast to previous findings, the lifetimes of turbulence in pipe flow do not diverge at a finite critical Reynolds number. All the available data indicate that turbulence in pipe flows decays, and that eventually the flow will always relaminarize. Similarly, lifetimes for Couette[18,19] flow and for a shear flow model[25] do not appear to diverge, suggesting that a finite lifetime of turbulence may be a universal property of this class of flows. The rapid exponential increase of lifetimes explains why the transient nature of turbulence has not been observed previously: to detect the decay of turbulence in a garden hose at a flow rate as low as 11 min^{-1} (Re = 2,400) would require a physical length of the tube of 40,000 km, about the Earth's circumference, and an observation time of almost 5 years. The dynamical connection between the turbulent and the laminar state implies that the flow can be relaminarized by infinitesimal perturbations in judiciously chosen directions. This implies in particular that turbulence control should be possible with minimal expenditures in energy.

Received 1 June; accepted 19 July 2006.

1. Nieuwstadt, F. J., Skrbek, L., Sreenivasan, K. R. & Donnelly, R. Turbulent convection at very high Rayleigh numbers. *Nature* 404, 837–840 (2000).
2. Grossmann, S. The onset of shear flow turbulence. *Rev. Mod. Phys.* 72, 603–618 (2000).
3. Hof, B. et al. Experimental observation of nonlinear travelling waves in turbulent pipe flow. *Science* 305, 1594–1598 (2004).
4. Reynolds, O. An experimental investigation of the circumstances which determine whether the motion of water shall be direct or sinuous and of the law of resistance in parallel channels. *Proc. R. Soc. Lond.* 35, 84–99 (1883).
5. Kerswell, R. R. Recent progress in understanding the transition to turbulence in a pipe. *Nonlinearity* 18, R17–R44 (2005).
6. Eckhardt, B., Schneider, T. M., Hof, B. & Westerweel, J. Turbulence transition in pipe flow. *Annu. Rev. Fluid Mech.* (submitted).
7. Brosa, U. Turbulence without strange attractor. *J. Stat. Phys.* 55, 1303–1312 (1989).
8. Faisst, H. & Eckhardt, B. Sensitive dependence on initial conditions in transition to turbulence in pipe flow. *J. Fluid Mech.* 504, 343–352 (2004).
9. Peixinho, J. & Mullin, T. Decay of turbulence in pipe flow. *Phys. Rev. Lett.* 96, 094501 (2006).
10. Shinbrot, T., Grebogi, C., Ott, E. & Yorke, J. A. Using small perturbations to control chaos. *Nature* 363, 411–417 (1993).
11. Drazin, P. G. & Reid, W. H. *Hydrodynamic Stability* (Cambridge Univ. Press, Cambridge, UK, 1981).
12. Faisst, H. & Eckhardt, B. Travelling waves in pipe flow. *Phys. Rev. Lett.* 91, 224502 (2003).
13. Eckhardt, B. & Mersmann, A. Transition to turbulence in a shear flow. *Phys. Rev. E* 60, 509–517 (1999).
14. Wedin, H. & Kerswell, R. R. Exact coherent solutions in pipe flow: travelling wave solutions. *J. Fluid Mech.* 508, 333–371 (2004).
15. Kadanoff, L. P. & Tang, C. Escape from strange repellers. *Proc. Natl Acad. Sci. USA* 81, 1276–1279 (1984).
16. Kantz, H. & Grassberger, P. Repellers, semi-attractors, and long-lived chaotic transients. *Physica D* 17, 75–86 (1985).
17. Hof, B. in *Proc. IUTAM Symp. on Laminar-Turbulent Transition and Finite Amplitude Solutions* (eds Mullin, T. & Kerswell, R. R.) 221–231 (Springer, Dordrecht, 2005).
18. Bottin, S. & Chaté, H. Statistical analysis of the transition to turbulence in plane Couette flow. *Eur. Phys. J. B* 6, 143–155 (1998).
19. Schmiegel, A. & Eckhardt, B. Fractal stability border in plane Couette flow. *Phys. Rev. Lett.* 79, 5250–5253 (1997).
20. Wygnanski, I. J. & Champagne, F. H. On transition in a pipe. Part 1. The origin of puffs and slugs and the flow in a turbulent slug. *J. Fluid Mech.* 59, 281–335 (1973).
21. Wygnanski, I. J., Sokolov, M. & Friedman, D. On transition in a pipe. Part 5. The equilibrium puff. *J. Fluid Mech.* 69, 283–304 (1975).
22. Hof, B., van Doorne, C. W. H., Westerweel, J. & Nieuwstadt, F. T. M. Turbulence regeneration at moderate Reynolds numbers. *Phys. Rev. Lett.* 95, 214502 (2005).
23. Rotta, J. C. Experimenteller Beitrag zur Entstehung turbulenter Strömungen im Rohr. *Ing. Archiv* 24, 258–281 (1956).
24. Schmiegel, A. *Transition to Turbulence in Linearly Stable Shear Flows*. PhD thesis, Philipps-Univ. Marburg (1999).
25. Moehlis, J., Faisst, H. & Eckhardt, B. A low-dimensional model for turbulent shear flows. *N. J. Phys.* 6, 56 (2004).

Supplementary Information is linked to the online version of the paper at www.nature.com/nature.

Acknowledgements This work was funded through a RCUK fellowship (B.H.), the Foundation of Fundamental Research on Matter (J.W.) and Deutsche Forschungsgemeinschaft (T.M.S. and B.E.). B.H. and J.W. thank R. Delfos for discussions and W. Tax and P. Tipler for technical assistance. We thank the Dorset Tube Company for supplying the precision pipe.

Author Information Reprints and permissions information is available at www.nature.com/reprints. The authors declare no competing financial interests. Correspondence and requests for materials should be addressed to B.H. (bjorn@reynolds.ph.man.ac.uk) or J.W. (j.westerweel@tudelft.nl).

EMATEM

Presentation Humphrey Spoor 33

Thank you for your attention.

…. has he finished….?

Thank you for your attention.

…. That was interesting….!

Discussion items for the future !

Is this all true ?

How to implement in a norm ?

resolution

minimum test volume

slew rate / time constant (excerpt from 2022)

Slew Rate (SR) versus Flow Change (FC)

When flow velocity profiles become dynamic, spatially and time dependent, it needs closer inspection.

Slew rate (SR)

The typical quantity in electronics, suitable to describe dynamic behaviour and reaction time of any device, is the slew-rate (SR). This quantity is directly related to the quality factor Q and the bandwidth B of amplifiers and oscillators (amplifiers with positive feedback). The slew-rate is defined as the maximum rate of change of a quantity that will be followed correctly by the system without distortion. Limitations in slew-rate capability can give rise to non-linear effects. In electronics the slew-rate is defined as:

$$SR_e\,[V/\mu s] \equiv \frac{\text{maximum voltage difference}\,[V]}{\text{rising time}\,[s]} = \left|\frac{dV_{max}(t)}{dt}\right| \qquad (1)$$

In hydrodynamics an analogue definition can be defined for rapid flow changes, where the maximum pressure rate fits in as follows ($\Delta V,I$ to $\Delta p,Q_V$ analogy):

$$SR_p\,[Pa/s] \equiv \frac{\text{maximum pressure variation}\,[Pa]}{\text{rising time}\,[s]} = \left|\frac{dp_{max}(t)}{dt}\right| \qquad (2)$$

For acoustic pulsations, i.e. the sudden pressure changes in flow, the Navier-Stokes equation can be applied. A simplification leads to the well-known Joukowski expression for acoustic shocks and waves in ducts

$$\Delta p = \rho\, c\, \tilde{u} = \frac{\rho\, c\, \tilde{Q}_V(t)}{A} \propto \Delta Q_V \qquad (3)$$

Intermezzo Joukowski linearization:

$$\Delta\left(\Delta\tilde{p}\right) = \tfrac{1}{2}\,\rho\,\Delta(c+\tilde{u})^2 = \tfrac{1}{2}\,\rho\,\Delta\left(c^2+\tilde{u}^2+2c\,\tilde{u}\right) \approx \rho\, c\, \tilde{u} = \frac{\rho\, c\, \tilde{Q}_V(t)}{A} \propto \Delta Q_V$$

where

ρ	= fluid density (kg/m³)
c	= sound velocity (m/s)
$\tilde{u}$	= flow velocity variations (m/s)
$Q_V(t)$	= volume flow variations (m³/s)
A	= cross sectional area (m²)

resolution
minimum test volume

slew rate / time constant (excerpt from 2022)

With the consideration of expression (3) in mind the hydraulic slew-rate can now be defined as

$$SR_q\left[m^3/s^2\right] \equiv \frac{\text{maximum allowable flow variation}\left[m^3/s\right]}{\text{rising time}\left[s\right]} = \left|\frac{dQ_V(t)}{dt}\right| \qquad (4)$$

which can be seen as the allowable limit for *flow accelerations (in fact **this** is "flow rate", in m^3/s^2 !)*. For the correlated *physical output frequency* (*) of a meter can be written,

$$f_{out}[Hz] = PC\left[p/m^3\right] * Q_V\left[m^3/s\right] \qquad (5)$$

using the definition for the primary constant PC (Geberkonstante), in pulse per volume.

(*) with *physical output frequency* is meant the measurement repetition frequency, given by the measurement principle and its construction, reciprocally related to the measurement time resolution. The PC gives the corresponding volume resolution.

If (5) is inserted into (4) then

$$SR_q\left[m^3/s^2\right] \equiv \left|\frac{dQ_V(t)}{dt}\right| = \frac{1}{PC}\frac{\Delta f_{out}}{\Delta t} \qquad (6)$$

containing the maximum sweep frequency variation $\Delta f_{out}/\Delta t$, specified by the manufacturer.

Flow Change (FC)

The comparison has to be made between this hydraulic slew-rate SR_q , being a characteristic of the flow meter, and the occurring flow change FC, i.e. the hydrodynamic response to rapidly changing process parameters, like opening or closing of valves, combined with surges from water hammer, edge tones, acoustic shocks, etc.

For the flow for sinusoidal opening / closing valves, $Q_V(t) = Q_V \sin(\omega t)$, the flow change can be written as

$$FC\left[m^3/s^2\right] \equiv \left|\frac{d}{dt}\left(Q_V \sin(\omega t)\right)\right| = \left|\omega\, Q_V \cos(\omega t)\right| = 2\pi\, f_{valve}\, Q_V \qquad (7)$$

with f_{valve} representing the commutation angular speed. The flow change FC << SR.